applied sciences

MDPI

Article

Model Modification of the Soil–Water Characteristic Curve of Unsaturated Weak Expansive Soil

Lina Ma [1,*], Jinran Guo [1,*], Dongfang Liang [2], Xiaogang Ding [1] and Yanjin Xue [1]

[1] School of Civil Engineering, Lanzhou Jiaotong University, Lanzhou 730070, China
[2] Department of Engineering, University of Cambridge, Cambridge CB2 1PZ, UK; dl359@cam.ac.uk
* Correspondence: malina@mail.lzjtu.cn (L.M.); guojinranvvip@163.com (J.G.); Tel.: +86-138-9314-0386 (L.M.)

Abstract: This study evaluates the impact of compaction on the soil–water characteristic curve of unsaturated remodeled weakly expansive soils by assessing changes in soil pore structure resulting from variations in compaction. The remodeled weakly expansive soil in the Xinjiang Hami area is taken as the research subject to investigate how compaction affects microscopic pore structure using mercury intrusion testing. Subsequently, mercury intrusion porosimetry is employed to examine pore structure and distribution patterns at different dry densities. Based on the capillary principle and experimental methods (filter paper method and pressure plate method test), modified soil–water characteristic curves are obtained by fitting them with a three-parameter model law. The results indicate that higher dry density leads to an increased air intake value and significantly reduces the total volume of large pores within samples. Both the Fredlund and Xing model and the three-parameter model effectively capture the influence of initial dry density on the development pattern of the soil–water characteristic curve.

Keywords: expansive soil; soil–water characteristic curve; matric suction; pore struct

Citation: Ma, L.; Guo, J.; Liang, D.; Ding, X.; Xue, Y. Model Modification of the Soil–Water Characteristic Curve of Unsaturated Weak Expansive Soil. *Appl. Sci.* **2024**, *14*, 7498. https://doi.org/10.3390/app14177498

Academic Editor: Tiago Miranda

Received: 16 July 2024
Revised: 16 August 2024
Accepted: 20 August 2024
Published: 24 August 2024

1. Introduction

Expansive soil, widely distributed worldwide, is a type of disastrous soil composed mainly of strong hydrophilic minerals in its clay composition. It exhibits significant characteristics such as "water absorption expansion and water loss shrinkage" and "reciprocating deformation" [1]. This poses a threat to various construction projects and their operations, with damages that are difficult to repair. As one of the crucial issues in the geotechnical engineering and geological engineering fields, expansive soil has caused severe problems during the early debugging stage of the Lanzhou–Xinjiang high-speed railway because of arch deformation caused by expansion and shrinkage, cracks, and over-consolidation [2], which seriously hindered its operation and development. Therefore, studying the soil–water characteristics of expansive soil is essential for providing technical support for designing new high-speed railways.

At present, many scholars have studied soil–water characteristics. Wang [3] studied the influence of dry density and sample water content on the macroscopic soil–water characteristics of loess. Ma [4] measured the soil–water characteristic curve of expansive soil under different concentrations of a NaCl solution in pores. Zhu [5] established a new model to predict the constitutive relationship between matric suction and water content in unsaturated soils. Chen [6] analyzed the influence of the initial void ratio on soil–water characteristics under high suction conditions through the soil–water characteristics test of compacted silt samples. Li [7] measured the soil–water characteristic curve of compacted loess silt with filter paper. The soil–water characteristic curve (SWCC) characterizes the relationship between matric suction and soil water content. It is widely used to describe the water state of soil according to the matrix suction of soil [8]. Some researchers used the SWCC to establish a thermodynamic frost heave model, which helped to evaluate the

mechanical properties of frozen soil [9,10]. It is very important to measure and calculate the SWCC accurately and efficiently when studying the characteristics of unsaturated soil and solving engineering problems. Zhou [11], Li [12], Hu [13], Ren [14], and others provided guidance for practical engineering by conducting indoor and outdoor test calculations and predicting soil–water characteristic curves. The change in influence suction is reflected in the strength and deformation characteristics of soil, and the strength and deformation characteristics of soil are reflected in the microscopic pore structure of soil. The suction in the pore matrix is generated by the pore water and air pressure on both sides of the curved liquid surface adsorbed on the soil particle skeleton [15–18]. However, previous studies have been limited to the macro factors affecting the soil–water characteristic curve. Studies on the hydraulic properties of soil should not ignore the influence of the microstructure, but it is difficult to meet the needs of scientific research and engineering because of the lack of micro-mechanism support.

The microstructure of soil plays a decisive role in all aspects of the properties of soil. The mechanical properties of soil can be understood as the macroscopic performance of the microstructure. Therefore, to solve the above problems, this paper will analyze the influence of compaction degree change on the microscopic pore volume content, pore size distribution, and pore shape of expansive soil through a mercury intrusion test. In summary, we used a pressure plate instrument (0–0.5 MPa) and the filter paper method (0–40 MPa) to generate the soil–water characteristic curve. Then, we applied the mercury intrusion method (capillary principle) to determine the theoretical calculation value of the soil–water characteristic curve and determined the reason why the theoretical calculation value of the soil–water characteristic curve was too small. Finally, the soil–water characteristic curve correction model of the mercury intrusion method (capillary principle) was proposed. Based on the soil–water characteristic curve, the model aims to analyze and evaluate the microscopic characteristics of soil and soil–water characteristics at the same time only through mercury intrusion technology, so as to simplify the test operation and shorten the test time.

2. Test Soil Samples

The expansive soil samples used in the test were taken from the 8-13 m drill core of a typical expansive arch section in the Hami area. The geological section is shown in Figure 1, and the expansive soil before and after encountering water is shown in Figure 2. The expansive soil used in the test is a typical Jurassic sedimentary rock, which is a mud-like structure with argillaceous cementation, poor diagenesis, and disintegration. It is a soft rock that is easy to soften in water and belongs to fully weathered–strongly weathered expansive soil. The basic characteristics of the soil samples are shown in Table 1. The soil sampling area is adjacent to the Tianshan Mountains. According to the nearby vegetation and groundwater seepage, there are abundant groundwater sources in this area, which provides the necessary conditions for the expansion deformation of expansive soil.

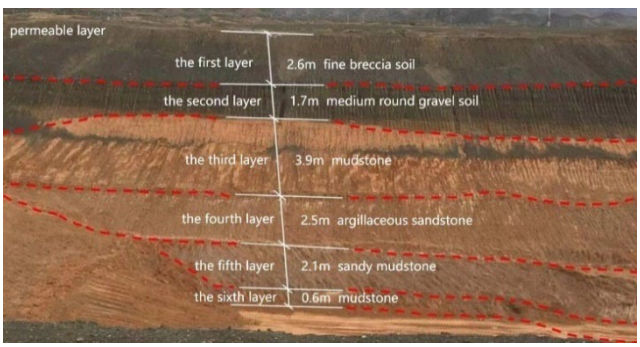

Figure 1. The geological section map of the borrow area.

Figure 2. Comparison of expansive soil before and after encountering water.

Table 1. Basic physical and physical indicators.

Index Property	Value
Specific gravity	2.74
Montmorillonite content	2.80%
Illite content	3.70%
Free expansion rate	57.00%
Cation exchange capacity	221.47 mmol·kg^{-1}
Liquid limit	40.87%
Plastic limit	20.02%
Plasticity index	20.85%

Note: According to the test results, the expansion grade is defined by the "Railway Engineering Geotechnical Classification Standard" (TB10077-2019), while the result is weak expansion soil.

The X-ray diffraction test, cation exchange capacity, free expansion rate, and liquid and plastic limit tests were carried out on the expansive soil taken from the site with reference to E.C.Childs and N.Collis George [19], Railway Engineering Geotechnical Test Procedure (TB10102-2023), and Railway Engineering Geotechnical Analysis Procedure (TB10103-2008).

3. Test Process

3.1. Mercury Intrusion Porosimetry Test

Mercury intrusion porosimetry (MIP) was first proposed by H.L. Ritter and L.C. Drake [20], while the mercury pressure test is based on mercury's non-moistness to solid surfaces. In this paper, it is assumed that the porous material is composed of cylindrical capillaries of various sizes. According to the lifting principle of liquid in the capillary, the microporous structure of the material is measured. Based on the Washburn Equation, the relationship between pressure P and capillary radius R for mercury is calculated as follows:

$$P = -\frac{2\sigma cos\theta}{R} \quad (1)$$

where P is the pressure of the intruded mercury (N·m^2), σ represents the surface tension of mercury (σ = 0.485 N·m^{-1}), θ is the wetting angle between the measured porous material and mercury, and R denotes the pore radius (nm). (The symbols appearing in this manuscript are re-annotated in Appendix A).

The test preparation had a dry density of 1.4~1.8 g/cm^3, and the expansion soil samples with equal intervals of 0.1 g/cm^3 were divided into five groups. Next, the specimens were cut into small pieces and put into a test tube filled with isopropyl. Each sample's internal moisture was converted into crystalline sublimation by vacuuming for 24 h. The samples were dried via lyophilization in liquid nitrogen to avoid changes in pore structure caused by water loss. Next, the dried samples were loaded into a dilatometer for low-pressure and high-pressure mercury intrusion tests, and then pore volume accumulation was generated.

3.2. Pressure Plate Method Test

In this experiment, the SWCC-150 Fredlund-type soil–water characteristic pressure gauge developed by the GCTS company in the United States was used. The water variable tube was calibrated before the test, and a clay plate with an air intake value of 5 bar was selected to measure the soil matric suction in the range of 0–0.5 MPa as a supplement to the low suction range of the filter paper method.

The pressure plate method test used hydraulic jacks to prepare ring knife samples with initial dry densities of 1.4, 1.5, 1.6, 1.7, and 1.8 g·cm^{-3}, respectively, while the clay plate with an intake value of 5 bar was selected for the test. The samples and clay plates were saturated. The suction path was 20→40→60→80→100→200→400 kPa, during which uninterrupted readings were performed. Before each reading, the bubbles were removed with a wash ear ball. After the water bodies on both sides were stabilized, step-by-step pressurization was performed. It took about 10 days to balance the suction value of each stage, and a set of parallel samples was prepared for the test.

3.3. Filter Paper Method Test

The paper filtration method followed the principle of thermodynamic equilibrium. The contact test method realized the equilibrium measurement of material suction through the water transfer between the filter paper and the soil. The non-contact test method measured the total suction through the balance between the filter paper and the water in the air. The test schematic is shown in Figure 3.

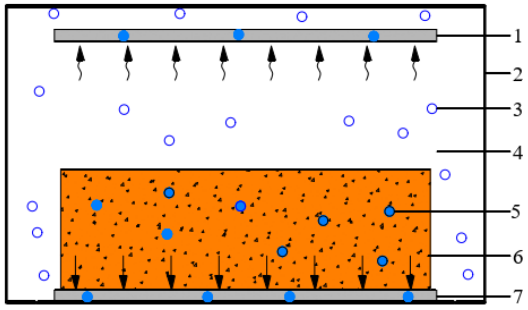

Figure 3. Profile of the principle of the filter paper test: 1 and 7 are filter paper, of which 1 is non-contact filter paper and 7 is contact filter paper; 2 is the sealing device; 3 is the gaseous migration of water molecules in the air; 4 is the air in the sealing device; 5 is the water molecule in the soil sample; 6 is the sample soil sample.

The filter paper method test adopted the domestic "double circle" brand NO. 203-type slow filter paper to measure the matric suction. The test steps were as follows: The filter paper was dried in the oven for 12 h and set aside. The soil sample was finely milled, passed through a 2 mm geo sieve, and then dried for 8 h in an oven at a constant temperature of 105 °C. Using a ring knife sampler and a hydraulic jack, five sets of standard ring knife samples with a diameter of 61.8 mm and a height of 20 mm were prepared. The samples had dry densities of 1.4 g·cm^{-3}, 1.5 g·cm^{-3}, 1.6 g·cm^{-3}, 1.7 g·cm^{-3}, and 1.8 g·cm^{-3}, with an initial moisture content of 4% and a gradient of 2%. A total of 10 groups of soil samples, with different moisture content, were prepared. An additional 2 groups of parallel specimens were prepared separately.

A circular sealing box was used as a test container. Notably, 3 pieces of filter paper were placed at the bottom of the box, with those on both sides acting as protective material. The protective filter paper had a slightly larger diameter than that of the ring knife. The middle filter paper was the test filter paper, and its diameter was the same as the diameter of the ring knife.

The matching sealing gasket was used for sealing treatment. It was placed in a test chamber maintained at a constant temperature of 25–27 °C for 10 days.

An electronic balance with an accuracy of 0.0001 g was used to measure the moisture content of filter paper quickly. Based on the filter paper method test, the soil–water characteristic curves of expansive soils with different densities in the high suction range (0.5–40 MPa) were obtained.

4. Analysis and Evaluation of the Pore Structure

The structural characteristics of the soil skeleton comprise the internal factors affecting the physical and mechanical properties of the soil and the soil–water characteristics. All kinds of soils generally develop micropores and microcracks, forming their own special microstructure [21]. Therefore, it is necessary to analyze the pore structure and pore distribution law of expansive soil under different degrees of compactness and study the fractal characteristics of pores. Based on the MIP test data, the pore distribution curves under different dry densities were obtained, as shown in Figure 4.

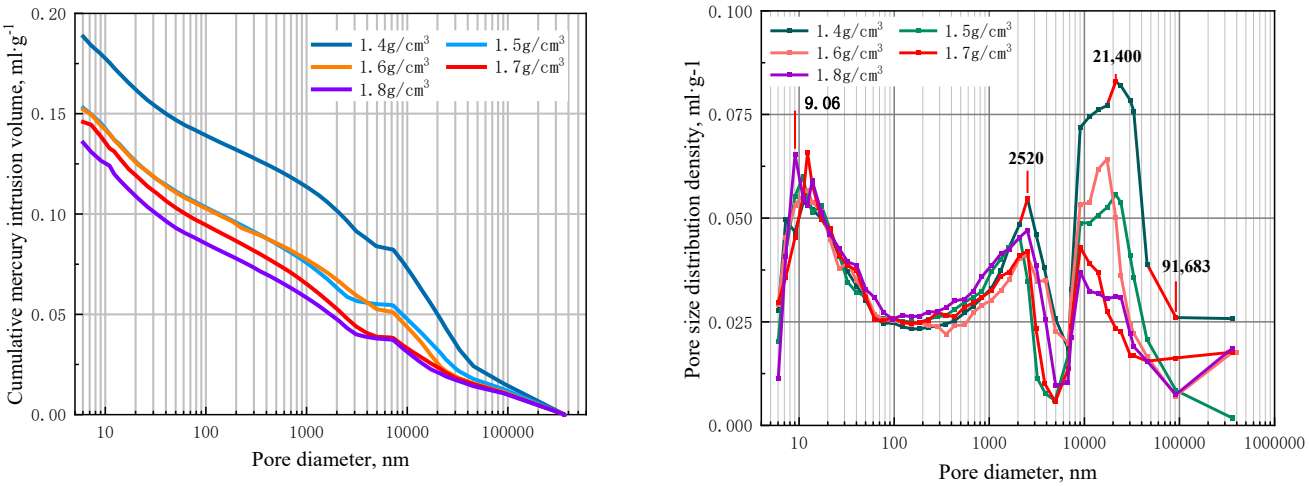

Figure 4. Pore distribution graphs at different dry densities. (**a**) Pore volume accumulation curve. (**b**) Pore distribution curve.

The sample's pore diameter ranges between 6 and 10^6 nm (Figure 4). The overall aperture distribution curve of the sample revealed three peaks (trimodal) distribution, corresponding to the aperture ranges of 6 to 77 nm (peak I), 550 to 3900 nm (peak II), and 6800 to 91,683 nm (peak III) (Figure 4b).

An increase in the dry density of the sample does not significantly influence the position and slope of the small pore part of the curve, while the peak and peak width fluctuations are small. The cumulative decrease is 86.25% within the $mL \cdot g^{-1}$ (1.4 $g \cdot cm^{-3}$) to 0.0114 $mL \cdot g^{-1}$ (1.9 $g \cdot cm^{-3}$) range. Notably, there is a significant peak decrease with a marked left shift, which is accompanied by a slight decrease in peak width, and a pore size distribution curve (PSD curve) that gradually tends to a double peak.

The soil skeleton inside the soil body is destroyed or recombined because of the increase in dry density of the expansive soil. This phenomenon causes significant changes in the pore structure, where some of the pore structure is destroyed, compacted, filled, or converted into other smaller diameter pores. Its impact on the pore volume content of the soil is shown in Figure 5. The total volume of the accumulated pores inside the expansive soil was reduced by 28.09%, while the cumulative reduction in total volume in large, medium, and small pores were 60.00, 12.36, and −3.16%, respectively. The volume of large pores decreased approximately linearly, which was obvious, while that of small pores increased. The destruction and reorganization of pore structure caused by the change in dry density of expansive soil significantly impacted the internal pore distribution and proportion of expansive soil.

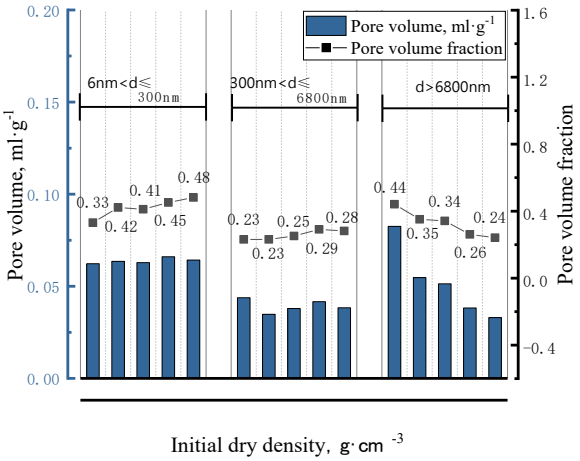

Figure 5. Influence of compaction on the pore content of expansive soil.

The above results indicated that an increase in the dry density of the sample generates a relatively linear content of the pores inside the mud rock. Notably, the sample's dry density had no significant effect on the pore content or particle size distribution of the small aperture (6 to 300 nm), while the total volume basically remained unchanged. Moreover, the sample's dry density had little effect on the pore content and particle size distribution of the mid-hole (300-6800 nm). The dry density of sample preparation had a significant impact on large pores (>6800 nm), while the volume content of large pores decreased significantly. Particularly, 6800~10^5 nm pores were most significantly affected by the dry density of the sample

5. Analysis of Soil–Water Characteristic Curves

Considering the known pore structure of the soil, the relationship between the matric suction and the pore diameter D can be obtained by the capillary principle, as shown in Equation (2). Then, the soil–water characteristic curve of rock and soil can be derived.

$$\psi = \frac{4Tcos\theta}{D} \tag{2}$$

where ψ is the matric suction of the soil (kPa), T is the unit of surface tension of the water (72.25 × 10^{-3} N·m^{-1}), θ is the contact angle between water and soil, and D is the pore diameter (nm).

The filter paper method test uses domestic "double-circle" brand NO. 203-type slow filter paper to measure substring suction and total suction force. This can be achieved using the filter curve equation in Equations (3) and (4).

The matric suction filter equation is as follows:

$$lg\psi = \begin{cases} -0.0767w + 5.493, w \le 47\% \\ -0.0120w + 2.470, w > 47\% \end{cases} \tag{3}$$

The total suction filter equation is as follows:

$$lgs = \begin{cases} -0.0700w + 5.257, w \le 41\% \\ -1.1940w + 51.321, w > 41\% \end{cases} \tag{4}$$

where s and w are the total suction force of the soil body (kPa) and the moisture content of the filter paper quality (%), respectively.

Considering that the results of the filter paper method are obviously affected by the environment in the low suction range, the suction value of 0–0.5 MPa is measured by the pressure plate method as a supplement. The characteristic curve of expansive soil water, obtained by the test method, is shown in Figure 6.

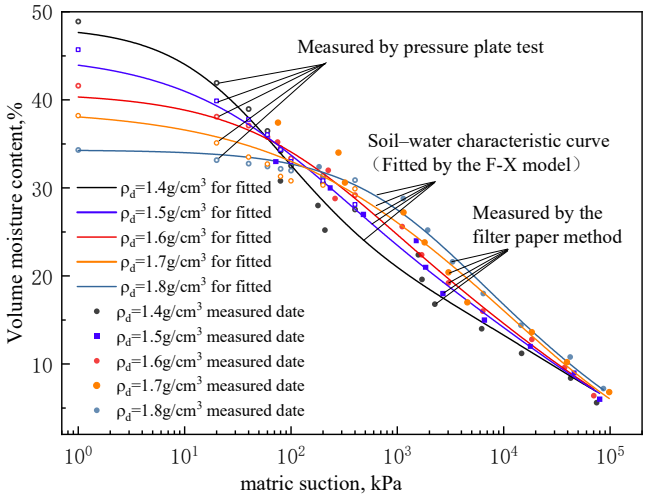

Figure 6. Soil–water characteristic curves.

Based on the characteristic curve of the expansive soil and soil water (Figure 6), it is evident that the soil matric suction exhibits a non-linear decrease, with varying degrees of increase with increasing dry density under the same volumetric water content conditions. When combined with the PSD curve, it can be considered that the increase in the initial dry density of the soil sample changes the pore structure and its distribution law, and the pore structure of the sample determines the suction force and is reflected in the soil–water characteristic curve. The increase in the sample's initial dry density results in a corresponding increase in the number and proportion of small pores. Notably, the sample as a whole exhibits a higher suction value, reflecting the pore structure characteristics of the soil.

In order to further verify the accuracy of the test results, three widely accepted typical SWCC models, namely, the Vangenuchten function (V-G), the Fredlund and Xing model (F-X), and the Gardner model, were used to fit the soil–water characteristic curve obtained by the test method.

Among them, the Fredlund and Xing fitting coefficient R^2 is above 0.980, which is not only better than both van Genuchten and Gardner models but is also more suitable for suction fit analysis of weakly expansive soil. The fitting parameters are shown in Table 2.

(a) The Fredlund and Xing model is as follows:

$$\theta = C(\psi)\frac{\theta_s}{\left\{\ln\left[e + (\psi/a)^n\right]\right\}^m} \tag{5}$$

where θ denotes the actual volume water content (%), θ_s is the saturated volumetric water content (%), a represents the fitting parameter related to the air-entry value of the soil (kPa), n is the fitting parameter related to the slope of the SWCC, m denotes the fitting parameter related to the residual water content of the soil, and e is the Euler number, 2.71828.

$$C(\psi) = \left[1 - \frac{ln(1 + \psi/C_r)}{ln(1 + 10^6/C_r)}\right] \tag{6}$$

where $C(\psi)$ is a correction factor, and C_r is the residual matric suction (kPa).

(b) Van Genuchten model is as follows:

$$\theta = \frac{\theta_s - \theta_r}{\left[\left(\frac{s}{b}\right)^n + 1\right]^m} + \theta_r \tag{7}$$

where b, n, and m are fitting parameters.

(c) The Gardner model is as follows:

$$\theta = \frac{\theta_s - \theta_r}{(\frac{S}{b})^n + 1} + \theta_r \quad (8)$$

where b and n are fitting parameters.

Table 2. SWCC model fitting SWCC parameters.

Initial Dry Density /g·cm^{-3}	F-X Model						V-G Model	Gardner
	θ_s	C_r/kPa	a	n	m	R^2	R^2	R^2
1.4	48.33	9900	26.75	0.872	0.686	0.980	0.988	0.946
1.5	45.16	11,960	70.23	0.582	0.915	0.992	0.961	0.948
1.6	40.82	16,693	205.74	0.623	0.936	0.994	0.978	0.966
1.7	38.93	19,902	1131.91	0.451	1.489	0.963	0.944	0.954
1.8	33.99	22,634	1564.89	0.736	1.012	0.992	0.985	0.964

6. Correction of the Soil–Water Characteristic Curve by the Mercury Intrusion Test

6.1. SWCC Three-Parameter Model Fitting

The movement of the water phase in unsaturated soil depends on soil particle size, mineral composition, pore distribution characteristics, temperature, and embossing degree. In some cases, for example, when soil moisture is affected by one or more factors, the SWCC is the only curve of soil moisture-base suction. However, it cannot be deduced from theoretical analysis according to the basic properties of soil. The movement of the water phase in unsaturated soil depends on soil particle size, mineral composition, pore distribution characteristics, temperature, and compaction degree.

Considering the existing typical SWCC equations, including V-G, F-X, the Gardner model, etc., the formula is complex, and there are many parameters. In order to explore the influence of mudstone compaction degree (dry density) on the SWCC, based on the test data obtained by filter paper method, the nonlinear fitting analysis of soil water characteristic test results was carried out by using origin software. Through multiple model selection attempts, it was found that the three-parameter model can express the data more accurately:

$$\theta = \alpha + \beta ln(\psi + \gamma) \quad (9)$$

6.1.1. Fitting Analysis of the Three-Parameter Model by Test Method

The soil–water characteristic curve, obtained by the pressure plate method (0~0.5 MPa) and the filter paper method (0~40 MPa), was fitted and analyzed using the three-parameter model shown in Equation (9), while the fitting information of each parameter under different dry densities was obtained, as shown in Table 3.

Table 3. Model fitting results.

ρ_d/(g·cm^{-3})	Fitting Parameters			R^2
	α	β	γ	
1.4	52.292	−4.173	1.043	0.974
1.5	52.688	−4.158	4.206	0.993
1.6	54.396	−4.284	19.769	0.996
1.7	56.912	−4.418	109.112	0.961
1.8	63.966	−4.646	411.742	0.991

The three-parameter logarithmic model has a fitting coefficient (R^2) that ranges between 0.974 and 0.996. Notably, the fitting parameters are significantly affected by dry density and are strongly correlated, indicating that the soil–water characteristic curve model has excellent applicability to the expansive soil in the Hami region of Xinjiang.

In order to analyze the influence of soil dry density on the soil–water characteristic curve, the linear/nonlinear fitting analysis of dry density was carried out on the fitting parameters α, β, and γ. The results are shown in Figure 7.

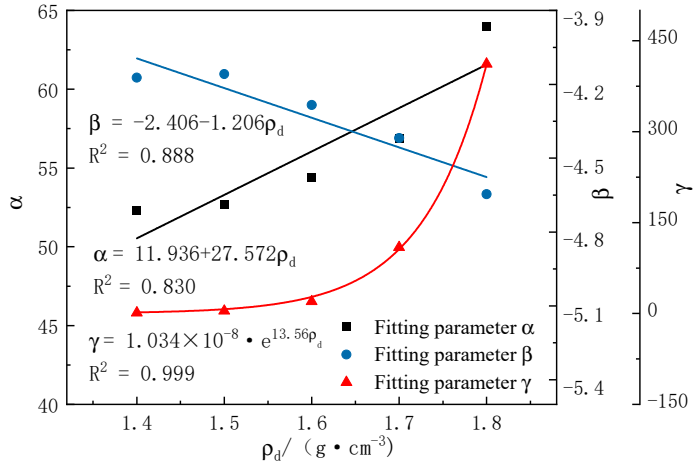

Figure 7. Profiles of the fitting parameters on dry density.

The relationships between α, β, and γ and the three-parameter model of the filter paper method are as follows:

$$\alpha = 11.936 + 27.572\rho_d \quad (10)$$

$$\beta = -2.406 - 1.206\rho_d \quad (11)$$

$$\gamma = 1.034 \times 10^{-8} \cdot e^{13.56\rho_d} \quad (12)$$

where ρ_d is the initial dry density of the soil.

Equations (10)–(12) were substituted into Equation (9), and a mathematical model of the soil–water characteristic curve containing only the initial dry density ρ_d of the expansive soil was obtained. Equation (13), which can predict and calculate the suction of the soil matrix under the condition of known soil volume moisture content and dry density, can be used for other characteristic analyses of rock and soil.

$$\theta_1 = 11.936 + 27.572\rho_d - (2.406 + 1.206\rho_d)ln(\psi_1 + 1.034 \times 10^{-8}e^{13.56\rho_d}) \quad (13)$$

where θ_1 is the volumetric moisture content of the filter paper method (%), and ψ_1 is matric suction measured for the filter paper method test (kPa).

6.1.2. Three-Parameter Model Fitting Analysis by the Mercury Intrusion Test

Based on the known pore structure of the soil in the mercury intrusion test, the suction force of the soil was calculated by the capillary principle in Equation (5). The fit analysis of the results was carried out by the three-parameter model of Equation (10), and the resulting fitting information of each parameter under different dry densities is shown in Table 4.

Table 4. Model fitting results.

ρ_d/(g·cm^{-1})	Fitting Parameters			R^2
	α	β	γ	
1.4	45.517	−4.182	−0.412	0.980
1.5	46.665	−4.124	0.524	0.993
1.6	43.783	−3.912	0.729	0.992
1.7	43.347	−3.860	3.887	0.995
1.8	39.131	−3.423	4.197	0.993

The three-parameter logarithmic model has a fitting coefficient (R^2) that ranges between 0.980 and 0.995, with a good fitting effect. The linear fitting analysis of the fitting parameters α, β, and γ for the dry density ρ_d was performed, and the results are shown in Figure 8.

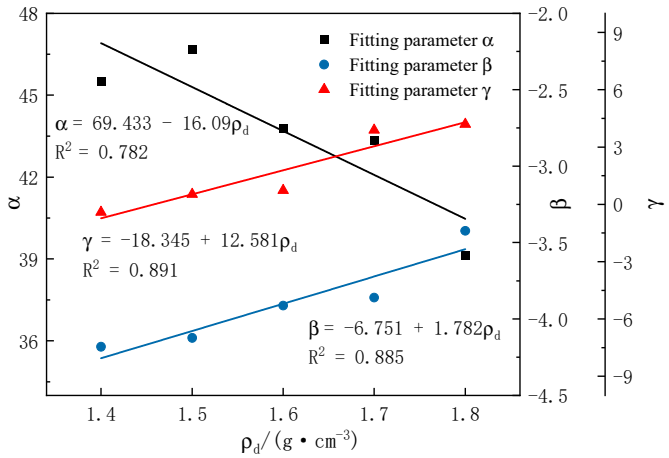

Figure 8. Profile of the fitting parameters on dry density.

The relationships between α, β, γ, and ρ_d of the three-parameter model of the mercury intrusion test are as follows:

$$\alpha = 69.433 - 16.09\rho_d \quad (14)$$

$$\beta = -6.751 + 1.782\rho_d \quad (15)$$

$$\gamma = -18.345 + 12.581\rho_d \quad (16)$$

Substituting Equations (14)–(16) into Equation (9) results in a mathematical model of the soil–water characteristic curve containing only the dry density of the expanding soil, as shown in Equation (17). Combined Equation (2) can be based on the known dry density and pore diameter of the soil, and the suction–volume moisture content curve of the soil matrix can be predicted and calculated as follows:

$$\theta_2 = 69.433 - 16.09\rho_d - (6.751 - 1.782\rho_d)\,ln(\psi_2 - 18.345 + 12.581\rho_d) \quad (17)$$

where θ_2 is the volumetric moisture content of the mercury intrusion test (%), and ψ_2 is the matric suction calculated based on the capillary principle for the mercury intrusion test (kPa).

It can be seen from Equation (17) that the soil–water characteristic curve of expansive soil is not a simple linear relationship with dry density, but the three parameters in the three-parameter model can be expressed by ρ_d. The correlation is high, indicating that the distribution of pore structure and pore size in expansive soil are closely related to the soil–water characteristic curve. Under the same volume of water content, the greater the dry density of mudstone, the more internal small pores, and the greater the matrix suction because of the presence of capillary force.

6.2. Correction of Soil–Water Characteristic Curves by the Capillary Principle

According to the above analyses, SWCC test values were obtained, based on the pressure plate method and the filter paper method, as well as the SWCC theoretical calculation value based on mercury intrusion porosimetry, as shown in Figure 9. There is consistency in the theoretical calculation and test values of the expansive soil–water characteristics obtained using mercury intrusion porosimetry and the filter paper method, respectively. The soil–water characteristic curve corresponding to the area with high pore size distribution density is steep, while the soil–water characteristic curve corresponding to the area with low pore size distribution density is slow. Moreover, the SWCC trend has a step-like

distribution under semi-logarithmic coordinates. The development trend in the soil–water characteristic curves, obtained by the two methods, is basically the same. However, the theoretical calculation values of matric suction under the same volumetric moisture content are less than the experimental values and increase with the increase in soil sample dry density.

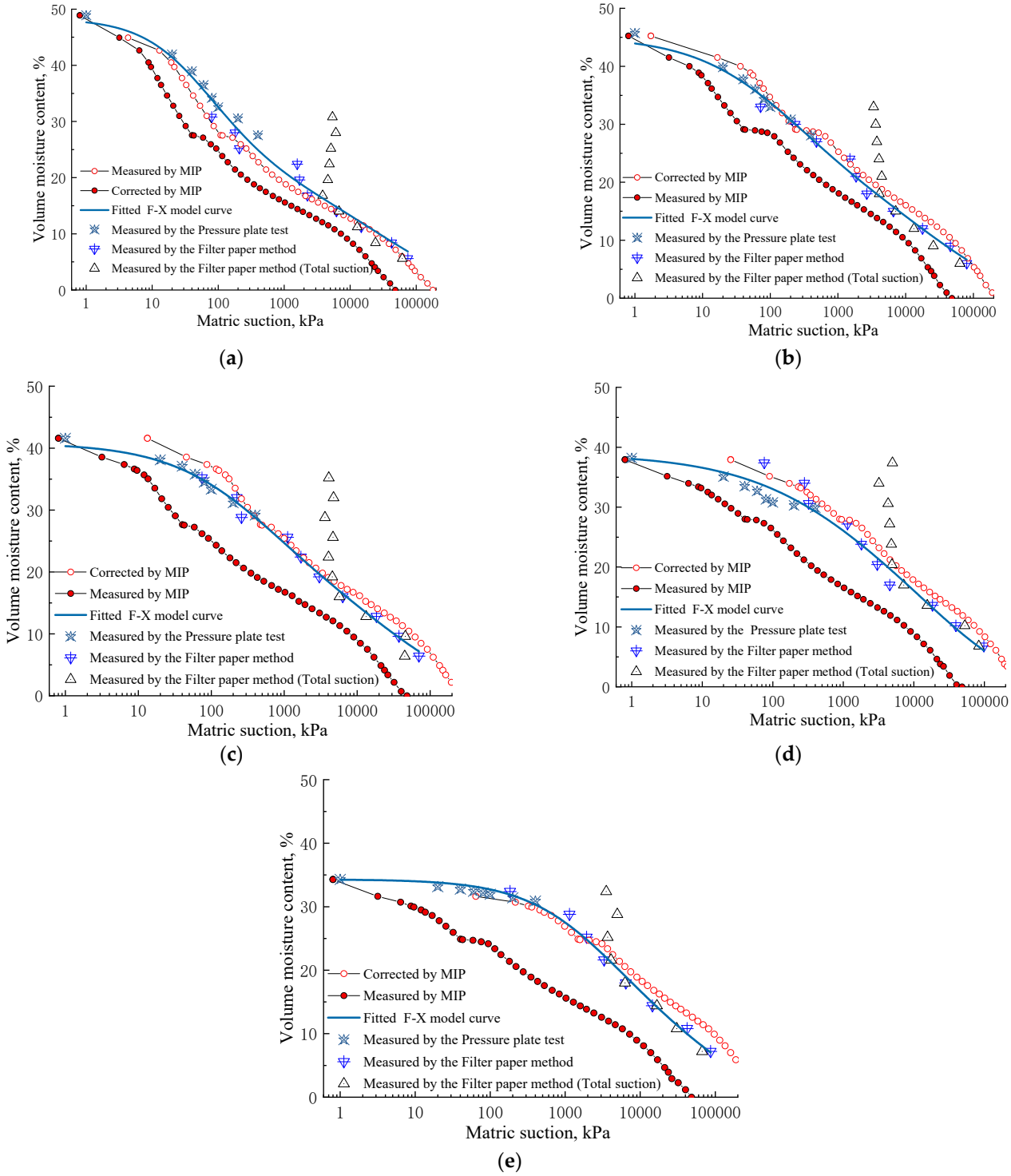

Figure 9. SWCC curves at different dry densities: (**a**) 1.4 g·cm^{-3}; (**b**) 1.5 g·cm^{-3}; (**c**) 1.6 g·cm^{-3}; (**d**) 1.7 g·cm^{-3}; and (**e**) 1.8 g·cm^{-3}.

This phenomenon is attributed to the following reasons: Firstly, the MIP test does not generate all the pore volume of the expansive soil. In addition, the minimum equivalent pore size that can be measured is 6 nm, while the minimum pore size that the geotechnical test water molecules can fill is 0.3 nm. From Equation (2), it is evident that the soil's suction force of is inversely proportional to the pore size, that is, the suction value generated by this part of the pore itself is very large. Secondly, the pore shape of the soil body is not completely in line with the spherical pore hypothesis, and the pores in the actual cohesive soil often have complex flat shapes (rhomboid-shaped). Notably, an increase in mercury pressure causes a continuous increase in the pore mercury medium, although it cannot be filled (the mercury pressure P cannot be infinitely increased). Zhang et al. [22] analyzed the fractal dimension of a soil body and found that an increase in the dry density of the sample resulted in a more complex spatial distribution morphology of the pores of the mudstone, and the farther the morphological characteristics of the pore surface of the material in space deviated from the smooth surface. Consequently, the two curves deviate, and the degree of deviation increases with the increase in dry density.

In order to realize the simultaneous analysis and evaluation of the microscopic properties and soil–water properties of soil using the mercury intrusion technique alone, the theoretical calculation of the SWCC was modified based on the filter paper method test value. Particularly, when the moisture content is $\theta_1 = \theta_2$, the theory should have $\psi = \psi_1$. Therefore, the corrected matric suction ψ can be obtained as follows:

$$\psi = \psi_1 = e^{\left(\frac{57.497 - 43.662\rho_d - (6.751 - 1.782\rho_d)ln(\psi_2 - 18.348 + 12.581\rho_d)}{-2.406 - 1.206\rho_d}\right)} - 1.034 \times 10^{-8} \times e^{13.56\rho_d} \quad (18)$$

The suction correction model of the mercury pressure method (capillary principle), based on the filter paper method, was obtained, as shown in Equation (18), while the correction curve is shown in Figure 8. This model allows efficient calculation and prediction of the suction of the soil matrix based on the microscopic pore structure, density state, and moisture content of a soil body

6.3. Correction Result Verification

To verify the correctness and applicability of the correction results of Equation (18), the results were verified using instruments proposed by Wang Xiaoqi et al. [23] and Ye Weimin et al. [24]. Wang Xiaoqi et al. used a stress-related soil–water characteristic curve pressure plate instrument (SDSWCC-H) to analyze the soil and water characteristics of Nanyang expansion soil in a certain stress state. Ye Weimin et al. studied the SWCC of weakly expansive soil on a slope of a highway in Hubei Province using the gas phase method and dialysis (liquid phase) method and predicted its relative permeability coefficient. The results are shown in Figure 10.

The Pearson correlation coefficient analysis values for testing and predicting matric suction were 0.955 [23] and 0.999 [24], respectively. The characteristic curve of expanding soil and soil water in the full suction range can be obtained by adopting the gas phase method and dialysis method (0.01–309 MPa). The soil–water characteristic curve of typical unsaturated soil is divided into boundary effect segments, transition segments, and unsaturated residual segments based on the intake value and residual suction value. The data shown in Figure 9 indicate that the suction force gap in the expansive soil matrix is nearly five quantitative intervals. The correction curve coincides with the test curve in the transition section, and the prediction result in the boundary effect segment is slightly higher than the measured value. Because of the experimental range limitation of the filter paper method, the non-saturated residual suction section cannot be predicted. Therefore, it is inferred that the prediction model proposed in this paper can better reflect the development law of the soil–water characteristic curve of the expansive soil transition section. Considering that there are few studies on expansive soils in this region, and differences

in soil properties across regions affect the model results, the universality of the modified model needs to be further verified.

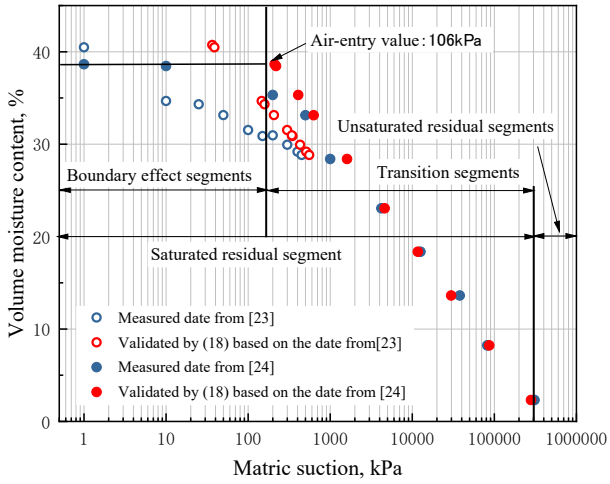

Figure 10. MIP-SWCC correction result validation [23,24].

7. Conclusions

In this paper, indoor experiments were performed to investigate the pore distribution, soil–water characteristic curve development, and change law of weakly expansive soil of high-speed rail foundations under different dry initial densities. The soil–water characteristic curves were verified and fitted using the F-X model and a three-parameter model. Based on the results, the soil–water characteristic curve correction model of the mercury intrusion test (capillary principle) was proposed. The main conclusions are as follows:

(1) As the dry density increased, the total volume of pores in the swelling soil decreased by about 28.09%, the total volume of large pores became obvious and decreased by 60%, the volume content of small pores increased, and the PSD curve of expansive soil gradually changed from trimodal to bimodal.

(2) The soil–water characteristic curve obtained by the capillary principle was always lower than the soil–water characteristic curve obtained by the test method. Four models were used to fit the soil–water characteristic curve law, and the three-parameter model with a better fitting effect was chosen to analyze the influence law of different dry densities with the soil–water characteristic curve. Based on the test method and the fitting curve of the pressure measurement method (capillary principle), a soil–water characteristic curve model that can describe the influence of soil dry density change was proposed.

(3) Based on the capillary principle, the soil–water characteristic curve correction model can better reflect the development law of the soil–water characteristic curve in the transition section. In actual engineering, soil pore structure and distribution characteristics and the soil–water characteristic curve can be obtained only through mercury intrusion porosimetry, which can simplify the test and shorten the time-consuming analysis.

(4) The modified soil–water characteristic curve model was tested using the experimental results obtained by previous researchers, and the correctness of the model was determined. However, because of the limitation of the test range, the model cannot predict the soil–water characteristic curve of the unsaturated residual suction section of expansive soil. In addition, expansive soil is widely distributed throughout the world, and the expansive soil used in this paper is specifically expansive mudstone, so the universality of the modified model must still be verified.

Author Contributions: Conceptualization, L.M.; methodology, L.M., X.D. and Y.X.; validation, L.M.; formal analysis, L.M. and J.G.; investigation, X.D.; resources, L.M.; data curation, J.G.; writing—original draft preparation, J.G.; writing—review and editing, J.G.; visualization, J.G.; supervision, L.M.; project administration, L.M. and D.L.; funding acquisition, L.M. and D.L. All authors have read and agreed to the published version of the manuscript.

Funding: This research was funded by Research Technology Priorities Program of China State Railway Group Co., Ltd., the grant number is K2021G025; Innovation Project of Young Scientific and Technological Talents in Lanzhou City, the grant number is 2023-QN-50; Natural Science Foundation of Gansu, the grant number is 22JR11RA161.

Data Availability Statement: The datasets used and analysed during the current study available from the corresponding author on reasonable request.

Conflicts of Interest: The authors declare no conflict of interest.

Appendix A

P is the pressure of the intruded mercury.
σ is the surface tension of the mercury.
$\theta_{(1)}$ is the wetting angle between the measured porous material and mercury.
R is the pore radius.
ψ is the matric suction of the soil.
T is the unit of the surface tension of water.
$\theta_{(2)}$ is the contact angle between the water and soil.
D is the pore diameter.
s is the total suction force of the soil body.
ω is the moisture content of the filter paper quality.
$\theta_{(5)}$ is the actual volumetric water content.
θ_s is the saturated volumetric water content.
a, b, and m are fitting parameters.
n is the Euler number.
e is a correction factor.
$C(\psi)$ is the residual matrix suction.
C_r is the fitting parameter.
α, β, and γ are the initial dry densities of the soil.
ρ_d is the dry density.
θ_1 is matric suction measured using the filter paper method test.
ψ_1 is the volumetric moisture content of the mercury intrusion test.
θ_2 is the matric suction calculated based on the capillary principle for the mercury intrusion test.

References

1. Cui, X.; Zhang, X.; Wang, Y. Research progress on measurement method, evolution law and control technology of subgrade humidity. *China J. Highw. Transp.* **2024**, *37*, 1–33. [CrossRef]
2. Wang, C. Study on Discriminant and Classification of Expansive Soil in Ballastless Track of High-Speed Railway. Master's Thesis, Lanzhou Jiaotong University, Lanzhou, China, 2018.
3. Wang, Y.; Li, T.; Lei, Y. Response of soil water characteristics of compacted loess to its pore structure. *Chin. J. Rock Mech. Eng.* **2024**, *41*, 1246–1255. [CrossRef]
4. Ma, T.; Yu, H.; Wei, C. Influence mechanism of physical and chemical effects on shrinkage characteristics of expansive soil. *Rock Soil Mech.* **2023**, *45*, 697–704. [CrossRef]
5. Zhu, S.; Li, S.; Jiang, Q. Soil-water characteristic curve model based on particle size distribution and film water. *J. Chang. River Sci. Res. Inst.* **2024**, 1–9. Available online: http://kns.cnki.net/kcms/detail/42.1171.TV.20240521.1647.014.html (accessed on 19 August 2024).
6. Chen, J.; Li, Z.; Han, Z. Effect of initial void ratio on soil-water characteristics of unsaturated soil under high suction. *Hydrogeol. Eng. Geol.* **2022**, *49*, 47–54. [CrossRef]
7. Li, Y.; Po, S.; Li, J. Effect of dry density on soil-water characteristic curve of unsaturated compacted loessial silt. *Bull. Sci. Technol.* **2021**, *37*, 94–98. [CrossRef]

8. Rahardjo, H.; Kim, Y.; Satyanaga, A. Role of unsaturated soil mechanics in geotechnical engineering. *Int. J. Geo Eng.* **2019**, *10*, 8. [CrossRef]
9. Li, X.; Zheng, S.-F.; Wang, M.; Liu, A.-Q. The prediction of the soil freezing characteristic curve using the soil water characteristic curve. *Cold Reg. Sci. Technol.* **2023**, *212*, 103880. [CrossRef]
10. Yang, H.-Q.; Zhang, L. Bayesian back analysis of unsaturated hydraulic parameters for rainfall-induced slope failure: A review. *Earth Sci. Rev.* **2024**, *251*, 104714. [CrossRef]
11. Zhou, F.; Zhao, W. Prediction of unfrozen water content in unsaturated frozen soil based on soil-water characteristic curve. *Rock Soil Mech.* **2024**, 1–9. [CrossRef]
12. Li, G.; Liu, Z.; Feng, S. Analytical solution of infiltration and slope stability analysis of single-layer soil cover under heavy rainfall conditions. *Chin. J. Geotech. Eng.* **2024**, 1–10.
13. Hu, J.; Jin, L.; Lv, Z. The dynamic response of unsaturated foundation is solved based on soil-water characteristic curve considering deformation effect. *Chin. J. Geotech. Eng.* **2024**, 1–11.
14. Ren, Q.; Wang, P.; Guo, H. Analysis of soil-water characteristic curve and freezing characteristic curve of unsaturated silty clay in seasonal frozen area. *Hydro Sci. Cold Zone Eng.* **2024**, *7*, 1–5.
15. Li, G.-X.; Li, X.-M. Seepage force and excess pore water pressure in soil mechanics. *Geotech. Eng. World* **2009**, *12*, 11–12.
16. Tang, Y.; Zhang, X.; Zhao, S.; Wang, J.; Zhou, N. Fractal study of saturated soft clay around tunnel under subway vibration load. *China Civ. Eng. J.* **2007**, 86–91.
17. Zhang, B.; Li, S. Determination of surface fractal dimension for porous media by mercury porosimertry. *Ind. Eng. Chem. Res* **1995**, *34*, 1383–1386. [CrossRef]
18. Zhang, Y.; Bing, H. Experimental study on the influence of freeze-thaw cycles on soil pore characteristics based on mercury intrusion method. *Glacier Geocryol.* **2015**, *37*, 169–174.
19. Childs, E.C.; Collis-George, N. The permeability of porous materials. In *Royal Society Series A, Mathematical and Physical Sciences*; Royal Society: London, UK, 1950; pp. 392–405.
20. Drake, L.C.; Ritter, H.L. Macropore-size distributions in some typical porous substances. *Ind. Eng. Chem. Anal. Ed.* **1945**, *17*, 787–791. [CrossRef]
21. Cinelli, G.; Tondeur, F.; Dehandschutter, B. Mapping potassium and thorium concentrations in Belgian soils. *J. Environ. Radioact.* **2018**, *184*, 127–139. [CrossRef]
22. Zhang, T.; Ma, L.; Zhang, R.; Wang, Q.; Li, J. Analysis of the influence of MIP-based compaction on the microstructure of "micro-swelling" remolded mudstone. *J. Eng. Geol.* **2019**, *27*, 717–722.
23. Wang, X.; Wang, S.; Cheng, M.; Li, X.; Zhou, C.; He, B. Experimental study on soil-water characteristic curve of expansive soil considering the influence of net normal stress. *Chin. J. Geotech. Eng.* **2018**, *40*, 235–240.
24. Ye, W.; Zhang, Y.; Zhou, X.; Xie, Q. Soil water characteristics and unsaturated permeability characteristics of weak expansive soil in a highway. *Chin. J. Undergr. Space Eng.* **2009**, *5*, 1585–1589.